Int. J. Electrochem. Sci., 12 **(2017)** 10981 – 10993, doi: 10.20964/2017.11.06

International Journal of ELECTROCHEMICAL SCIENCE
www.electrochemsci.org

Synthesis and Characterization of Pitch-Coated $Li_2Mn_xFe_{1-x}SiO_4$/C Composite Cathode Material for Lithium-Ion Batteries

Ho-Ming Cheng[1], Hong-Gen Dai[2], Fu-Ming Wang[3,4,], Pi-Chuen Tsai[2] and Wei-Ren Liu[5]*

[1] Department of Materials Science and Engineering, National Taiwan University of Science and Technology, Taipei, Taiwan
[2] Graduate Institute of Material Science and Green Energy Engineering, National Formosa University, Yunlin, Taiwan
[3] Sustainable Energy Center, National Taiwan University of Science and Technology, Taipei, Taiwan, 43, Sec. 4, Keelung Rd., Taipei, 106, Taiwan
[4] Graduate Institute of Applied Science and Technology, National Taiwan University of Science and Technology, Taipei, Taiwan
[5] Department of Chemical Engineering, R&D Center for Membrane Center, Chung Yuan Christian University, Chungli, Taiwan
[*]E-mail: mccabe@mail.ntust.edu.tw

Received: 25 June 2017 / *Accepted:* 21 August 2017 / *Published:* 12 October 2017

In this study, two cathode materials were synthesized ($Li_2Mn_{0.5}Fe_{0.5}SiO_4$ and $Li_2Mn_{0.2}Fe_{0.8}SiO_4$). The intrinsic characteristics and electrochemical performance of these materials were investigated. These silicate cathode materials have several advantages such as high safety, low cost, low environmental toxicity, and high theoretical energy density. However, they have some drawbacks that must be addressed, including low electronic conductivity and low ionic diffusivity, which limit their practical application in lithium-ion batteries. The $Li_2Mn_xFe_{1-x}SiO_4$/C composite materials were prepared using the sol–gel method. The X-ray diffraction patterns of the synthesized $Li_2Mn_xFe_{1-x}SiO_4$/C composite materials exhibited favorable crystallinity. Pitch was coated on the synthesized composite materials to improve their electronic conductivity. Raman spectroscopy confirmed the high graphitization of the carbon coatings. The discharge capacity of the pitch-coated $Li_2Mn_{0.2}Fe_{0.8}SiO_4$/C ($Li_2Mn_{0.2}Fe_{0.8}SiO_4$/C/pitch) cathode was 183 mAh g^{-1} delivered in the first cycle at a rate of 0.1 C. The battery cycle retention was 85% after 30 cycles, demonstrating an excellent cycle life compared with those reported in previous studies. These cathode materials have high potential for application in lithium-ion batteries.

Keywords: lithium ion battery, sol-gel method, orthosilicate cathode, pitch, graphitization

1. INTRODUCTION

Lithium-ion batteries have been widely used as power sources in various portable electronic devices. One of the important concerns that remain to be addressed is the improvement of the energy density of the cathode material. A family of dilithium transition metal orthosilicates (Li_2ASiO_4, A = Mn, Fe, Co, Ni) have been suggested to be promising cathode materials because of their ability to deliver more than one Li^+ during charging and discharging [1]. It gives lithium-ion batteries a high theoretical energy density (nearly 330 mAh g^{-1}) [2] compares with the conventional cathode ($LiCoO_2$ or $LiMn_2O_4$), and the strong Si–O covalent bonds provide stable thermal stability and thus prevent O_2 release during cycling [3]. Moreover, the Li_2ASiO_4 have other appealing characteristics such as low cost [2], environmental benignity [4], and natural abundance [4]. However, these cathode materials have inherent poor electronic conductivity and low ionic diffusivity because the AO_4 tetrahedra (where A = Fe, Mn, Co, or Ni) are surrounded by the insulating SiO_4 tetrahedra [5]. For example, the electronic conductivity of Li_2FeSiO_4 and Li_2MnSiO_4 is reported to be of the order 10^{-14} [5] and 10^{-16} [6] S cm^{-1} at room temperature, respectively. The electronic conductivity of Li_2ASiO_4 has been demonstrated to be significantly lower than that of $LiFePO_4$. These drawbacks severely restrict the capacity, rate capability, and cyclability of these materials and thus limit their practical application in lithium-ion batteries. To date, numerous carbon sources have been used to enhance the electronic conductivity of Li_2ASiO_4 materials, such as carbon nanospheres [7], carbon nanotubes [8], reduced graphene oxide [9], and graphene oxide [10,11]. Capacity fading is also a common shortcoming of Li_2ASiO_4-based materials. Their poor cyclability originates from the formation of two-dimensional Li-layered Li_2ASiO_4 polymorphs, which are unstable upon full delithiation because of layer exfoliation and result in an amorphous structure. In situ X-ray diffraction (XRD) revealed the loss of intensity of Bragg diffraction during first oxidation, and this intensity is not recovered after the reduction [12].

Recently, a Li_2MnSiO_4 cathode material with a theoretical capacity of 333 mAh g^{-1} was reported [13]. During oxidation, the number of short Mn–O bonds in the MnO_4 tetrahedron decreases with an increase in the Mn valance state, whereas the long Mn–O bonds remain invariant [11]. In addition, the serious local distortions around the Mn^{2+} polyhedron upon delithiation lead to irreversible structural deterioration. X-ray absorption near edge spectroscopy was used to examine the Li_2ASiO_4 materials with Mn and Fe substitutions [14]. The results revealed that the local structure around the Mn ion altered from having tetrahedral to octahedral coordination during cycling, whereas Fe ions remained in their tetrahedral coordination. The structural site transformation of Mn ions plays an important role in the degeneration of cycle life performance. Therefore, the structural change of Li_2MnSiO_4 causes significantly voltage decay and capacity fading than the Li_2FeSiO_4 [15]. A study reported that the $Pmn2_1$ and Pmnb polymorphs of Li_2MnSiO_4 transformed into the anamorphous phase during the first Li^+ extraction and that the crystallinity was not recovered after subsequent reduction processes [16]. The aforementioned irreversible behaviors are most likely responsible for the poor cycle life of Li_2MnSiO_4. A ^6Li magic angle spinning–nuclear magnetic resonance spectrum enables the local environment around Li sites in Li_2MnSiO_4 and Li_2FeSiO_4 to be determined [17]. The spectra revealed broad spinning-sideband powder patterns, which reflect the arrangement of the paramagnetic Mn and Fe ions within the first cation coordination shell around Li. Each Mn in the Li–O–Mn bond

results in a negative shift of −20 to −40 ppm to the isotropic hyperfine ^{6}Li shift. The changes in the local environment of Fe in the Li_2FeSiO_4/C material were reversible, and the Mössbauer parameters remained unchanged after the first cycle [14]. Structural parameters obtained using extended X-ray adsorption fine structure revealed that the local environment of Fe was preserved after the cycle, with only a small relaxation in the structure, which maintained the life of the Li_2FeSiO_4 [18]. For improving the poor cyclability of Li_2MnSiO_4, modification with Fe-substituted Li_2MnSiO_4 material ($Li_2Fe_yMn_{1-y}SiO_4$) is suggested because Fe plays a key role in stabilizing the formation energies of $Li_2Fe_yMn_{1-y}SiO_4$ [19]. Density functional theory calculations predicted Li_2MnSiO_4 structures with a $Pmn2_1$ space group to collapse when Li ions are extracted, and $Li_2Mn_{0.5}Fe_{0.5}SiO_4$ is expected to remain stable with the extraction of up to 1.5 Li atoms per formula unit [3]. Some studies have used the partial substitution of Mn with Fe to improve the electrochemical performance of Li_2MnSiO_4. $Li_2(Fe_{1-x}Mn_x)SiO_4$ (x = 0, 0.3, 0.5, 0.7, 1) samples have been successfully synthesized using a citric acid assisted sol–gel route [20], solid state reaction [21], hydrothermal reaction [22], and the Pechini process [23].

Pitch is a common carbon source in our daily life. It contains abundant sp^2-hybridized carbon structures, and its structure is quite similar to that of graphene [24]. This results in good electronic conductivity in the carbon that it is obtained from pitch. Pitch as a carbon resource has been used for synthesizing olivine phosphate materials [25] and Li_2FeSiO_4 [26]; however, according to our review of relevant literature, pitch has not been used in the synthesis of $Li_2Fe_yMn_{1-y}SiO_4$ before.

In this study, two materials ($Li_2Mn_{0.5}Fe_{0.5}SiO_4$/C/pitch and $Li_2Mn_{0.2}Fe_{0.8}SiO_4$/C/pitch) were synthesized, and their crystallinity, electrochemical performance, and potential applications were compared. Moreover, how pitch coating enhanced electronic conductivity and electrochemical performance was also studied.

2. EXPERIMENT

To synthesize $Li_2Mn_{0.5}Fe_{0.5}SiO_4$/C and $Li_2Mn_{0.2}Fe_{0.8}SiO_4$/C, lithium acetate ($LiCH_3COO$), ferric citrate ($C_6H_5FeO_7$), manganese acetate ($Mn(CH_3COO)_2$), and TEOS ($Si(OC_2H_5)_4$) were used as starting materials and glucose ($C_6H_{12}O_6$) was employed as the chelating agent. All chemicals were purchased from Sigma-Aldrich Co, USA.

The concentrations of $Li_2Mn_xFe_{1-x}SiO_4$ sol precursor and glucose, prepared in deionized (DI) water, were 0.15 and 0.075 M, respectively. Stoichiometric amounts of the starting materials and chelating agents were weighed and mixed, and the mixed powder was then dissolved in DI water in a flask. The flask was immersed in an oil bath and then heated and stirred on a hot plate at 60 °C. After a reaction time of 23 h, the brown-colored wet gel was poured into a beaker and dried in a vacuum oven at 120 °C overnight. The dried gel was scraped and then placed in a crucible, which was calcined in a tube furnace filled with an N_2 atmosphere (heating rate 10 °C min^{-1}). The sintering temperature was 650 °C with a holding time of 10 h. After natural cooling, the black-colored product was ground into a fine powder using a mortar and pestle.

Conductive carbon was coated on the as-synthesized $Li_2Mn_xFe_{1-x}SiO_4/C$ to improve its conductivity and discharge capacity, instead of being coated in situ with carbon from the chelating agent. In this study, pitch was used as a carbon source in the postcarbon coating route. The $Li_2Mn_xFe_{1-x}SiO_4/C$ powder was coated with 30 wt% of pitch. An appropriate concentration of the as-synthesized $Li_2Mn_xFe_{1-x}SiO_4/C$ powder was first dispersed in the diluted acetone solution in a beaker. In addition, a moderate quantity of pitch was weighed and dispersed in another beaker in diluted acetone solution. Both beakers were agitated in an ultrasonic cleaner for 30 min. Subsequently, the two suspensions were mixed together and then further ultrasonically agitated for 30 min. The resultant mixture was stirred on a hot plate for 10 h, and the product was filtered out using vacuum filtration.

After the composite was dried overnight in a vacuum oven at 100 °C, the treated composite was scraped and then placed in a crucible, which was calcined in a tube furnace filled with an N_2 atmosphere (heating rate 5 °C min^{-1}). The sintering temperature was first increased to 180 °C for 5 h and then further increased to 600 °C for another 1 h. After natural cooling, the black-colored product was ground into a fine powder using a mortar and pestle.

The crystal structure and surface morphology of the powder was then studied using XRD and scanning electron microscopy (SEM). Energy-dispersive spectroscopy was used to compare the actual stoichiometric ratio of Mn:Fe:Si with the designed elemental amount in the synthesized samples. The carbon content and degree of graphitization of the carbon coating were determined separately by using elemental analysis (EA) and Raman spectroscopy. The thermal reactions related to the heating temperature of the pitch-coated $Li_2Mn_xFe_{1-x}SiO_4/C$ samples were studied by using differential scanning calorimetry (DSC).

The cathode electrode was composed of an active material (80 wt%), poly(vinylidene) fluoride (PVdF, 8 wt%) as a binder, conductive carbon KS-6 (7 wt%), and Super P (5 wt%). PVdF was first dissolved in 2 mL of N-methyl-2-pyrrolidonein in a polyethylene bottle. After the PVdF was thoroughly dissolved, the other materials and two zirconia beads were added to the bottle. The slurry was ball-milled using a mechanical stirrer for 2 h. The zirconia beads were then removed, and the slurry was poured onto an aluminum foil sheet and spread using a doctor blade film coating machine. Subsequently, the coated electrode sheet was dried overnight in a vacuum oven at 100 °C. After the electrode sheet was rolled using a rolling machine, the sheet was cut into small circular pieces (1.3 cm diameter). The small circular electrodes were used as cathodes, a porous Celgard 2320 film was used as a separator, and lithium metal was used as the anode. The electrolyte was $LiPF_6$ (1.0 M) dissolved in an ethylene carbonate/propylene carbonate/diethyl carbonate (3:2:5 in volume) mixed solvent.

The electrode materials were tested by assembling CR2032 coin-type cells with potentials ranging from 1.5 to 4.8 V, with a constant current rate of 0.0625 C on the battery test equipment (U-BIC). Cyclability tests comprised 30 cycles at a current rate of 0.0625 C.

The current response profile was measured using a cyclic voltammegram (CV) method on a potentiostat (Biologic VMP3). The voltage range was between 1.5 and 5.0 V, and the scan rate used was 0.1 mV s^{-1}. Moreover, electrochemical impedance spectroscopy (EIS) experiments were performed on the pitch-coated $Li_2Mn_{0.5}Fe_{0.5}SiO_4/C$ ($Li_2Mn_{0.5}Fe_{0.5}SiO_4/C$/pitch) and $Li_2Mn_{0.2}Fe_{0.8}SiO_4/C$ ($Li_2Mn_{0.2}Fe_{0.8}SiO_4/C$/pitch) cathode electrodes at 0% state of charge (SOC) after the cells were charged and discharged for five cycles. The frequency range was between 1M to 10

mHz, and the amplitude of the sinusoidal wave was 5 mV. All the used materials in this manuscript are arranged and named in Table 1.

Table 1 Used materials of this research.

	Used materials	**Abbreviated titles**
1	Starting material: $LiCH_3COO$, $C_6H_5FeO_7$, $Mn(CH_3COO)_2$, $Si(OC_2H_5)_4$, $C_6H_{12}O_6$	$Li_2Mn_{0.5}Fe_{0.5}SiO_4/C$
2	Starting material: $LiCH_3COO$, $C_6H_5FeO_7$, $Mn(CH_3COO)_2$, $Si(OC_2H_5)_4$, $C_6H_{12}O_6$	$Li_2Mn_{0.2}Fe_{0.8}SiO_4/C$
3	Starting material: $LiCH_3COO$, $C_6H_5FeO_7$, $Mn(CH_3COO)_2$, $Si(OC_2H_5)_4$, $C_6H_{12}O_6$ Carbon source: pitch	$Li_2Mn_{0.5}Fe_{0.5}SiO_4/C$/pitch
4	Starting material: $LiCH_3COO$, $C_6H_5FeO_7$, $Mn(CH_3COO)_2$, $Si(OC_2H_5)_4$, $C_6H_{12}O_6$ Carbon source: pitch	$Li_2Mn_{0.2}Fe_{0.8}SiO_4/C$/pitch

3. RESULTS AND DISCUSSION

Figure 1 presents the XRD patterns of four composite cathode materials. The crystallinity of all materials was favorable, and pitch coating did not affect the crystallinity of the coated $Li_2Mn_{0.5}Fe_{0.5}SiO_4/C$ and $Li_2Mn_{0.2}Fe_{0.8}SiO_4/C$. The XRD spectra also revealed that the orthorhombic crystal structure and $Pmn2_1$ space group were composed of all materials, which is compatible with the results of previous studies [27,28].

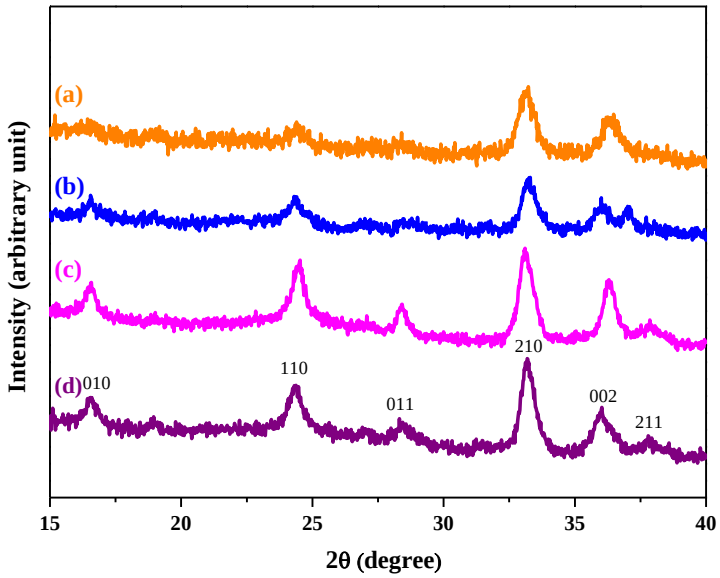

Figure 1. X-ray diffraction pattern of (a) $Li_2Mn_{0.5}Fe_{0.5}SiO_4/C$, (b) $Li_2Mn_{0.2}Fe_{0.8}SiO_4/C$, (c) $Li_2Mn_{0.5}Fe_{0.5}SiO_4/C$/pitch, and (d) $Li_2Mn_{0.2}Fe_{0.8}SiO_4/C$/pitch cathode materials

Figure 2 presents the SEM particle images of the four composite materials. All the materials were composed of irregularly shaped secondary particles. The $Li_2Mn_{0.5}Fe_{0.5}SiO_4/C$ and

$Li_2Mn_{0.5}Fe_{0.5}SiO_4$/C/pitch materials had a secondary particle size of approximately 10–60 μm. In addition, the $Li_2Mn_{0.2}Fe_{0.8}SiO_4$/C and $Li_2Mn_{0.2}Fe_{0.8}SiO_4$/C/pitch materials had a secondary particle size of approximately 10–50 μm. These images indicated that the primary particles commonly aggregate together in all materials.

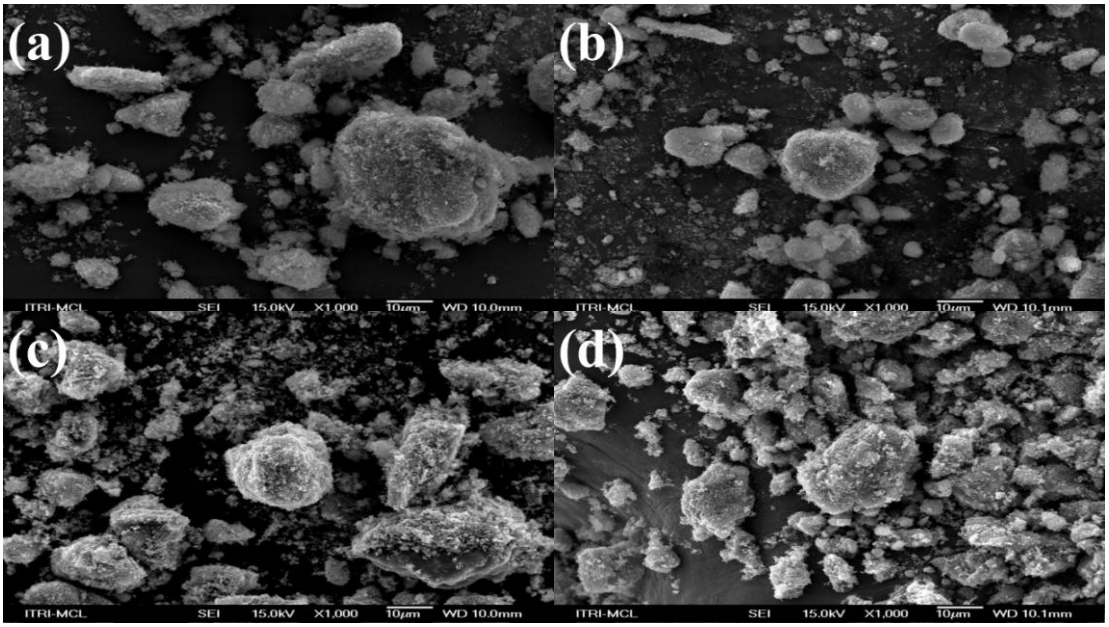

Figure 2. SEM images of (a) $Li_2Mn_{0.5}Fe_{0.5}SiO_4$/C, (b) $Li_2Mn_{0.2}Fe_{0.8}SiO_4$/C, (c) $Li_2Mn_{0.5}Fe_{0.5}SiO_4$/C/pitch, and (d) $Li_2Mn_{0.2}Fe_{0.8}SiO_4$/C/pitch composite materials.

Table 2 presents the results of the carbon content analysis of all the materials. These results were obtained using EA. The as-synthesized $Li_2Mn_{0.5}Fe_{0.5}SiO_4$/C and $Li_2Mn_{0.2}Fe_{0.8}SiO_4$/C contained 12.29 and 13.56 wt% carbon, respectively, whereas the $Li_2Mn_{0.5}Fe_{0.5}SiO_4$/C/pitch and $Li_2Mn_{0.2}Fe_{0.8}SiO_4$/C/pitch electrodes contained 43.35 and 39.58 wt% of carbon, indicating that pitch coating increased the carbon content to approximately 40 wt%. The inactive elements in the electrode had been eliminated, which was in accordance with the calculation of the theoretical energy density.

Table 2. Carbon content of various active materials we synthesized. The data were acquired from the results of EA experiments.

Sample	Carbon Content (%)
$Li_2Mn_{0.5}Fe_{0.5}SiO_4$/C	12.29 %
$Li_2Mn_{0.2}Fe_{0.8}SiO_4$/C	13.56 %
$Li_2Mn_{0.5}Fe_{0.5}SiO_4$/C/pitch	43.35 %
$Li_2Mn_{0.2}Fe_{0.8}SiO_4$/C/pitch	39.58 %

Figure 3 presents the Raman spectra of the four composite materials. The wavelength of the Raman excitation laser was 785 nm. The Raman shift ranged between 750 and 2000 cm^{-1}. The gray,

green, and red lines in Fig. 3 correspond to the measured Raman data, Voigt fitting curves for constituent bands, and resulting fits of carbon, respectively. The Raman spectrum of graphite mainly comprises the D (disorder, 1350 cm^{-1}) and G (graphite, 1580 cm^{-1}) bands, indicating the presence of disordered graphite and crystalline graphite in the sample [29]. The intensity ratio [I(D)/I(G)] of these two peaks was inversely proportional to the quality of graphite, and this value is widely used to evaluate the graphite crystallinity of samples. In addition to the two major Raman bands corresponding to graphite, the spectrum exhibited three minor Raman resonance bands. These three weak Raman peaks indicate information regarding the ratio of sp^2:sp^3 bonds (I), graphitic lattice defects (D'), and amorphous carbon content (D"). The peaks were denoted I, D', and D'' Raman modes and were located at approximately 1220, 1510, and 1620 cm^{-1}, respectively [30,31]. The $Li_2Mn_{0.5}Fe_{0.5}SiO_4$/C sample (Fig. 3a) exhibited an extremely weak Raman spectrum. Similarly, the Raman spectrum of the in situ carbon coating on the $Li_2Mn_{0.2}Fe_{0.8}SiO_4$/C sample (Fig. 3b) resulting from the chelating agent was also unclear. The characteristic D and G peaks in Figs. 3a and 3b were carefully identified, and the D/G ratio was calculated to be 0.850 and 1.320, respectively. Conversely, the pitch-coated materials had significantly more distinguishable D and G peaks. The D/G ratios were enhanced to 0.571 and 0.769 (Figs. 3c and 3d) in the $Li_2Mn_{0.5}Fe_{0.5}SiO_4$/C/pitch and $Li_2Mn_{0.2}Fe_{0.8}SiO_4$/C/pitch materials. The lower D/G ratios indicated the more favorable electronic conductivity of the composite materials, thus demonstrating that pitch is an excellent carbon source for ex situ conductive graphite coating modification.

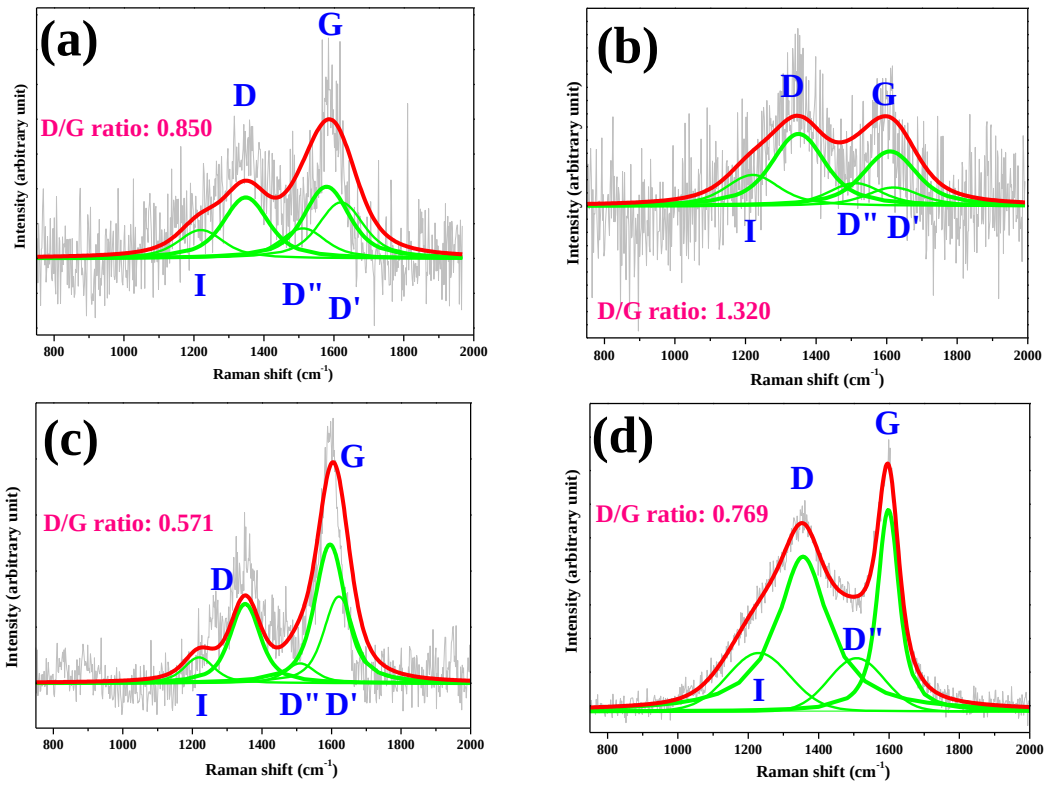

Figure 3. Raman spectra of (a) $Li_2Mn_{0.5}Fe_{0.5}SiO_4$/C, (b) $Li_2Mn_{0.2}Fe_{0.8}SiO_4$/C, (c) $Li_2Mn_{0.5}Fe_{0.5}SiO_4$/C/pitch, and (d) $Li_2Mn_{0.2}Fe_{0.8}SiO_4$/C/pitch composite materials. The signals of I, D, D', D", and G Raman modes were also indicated nearby.

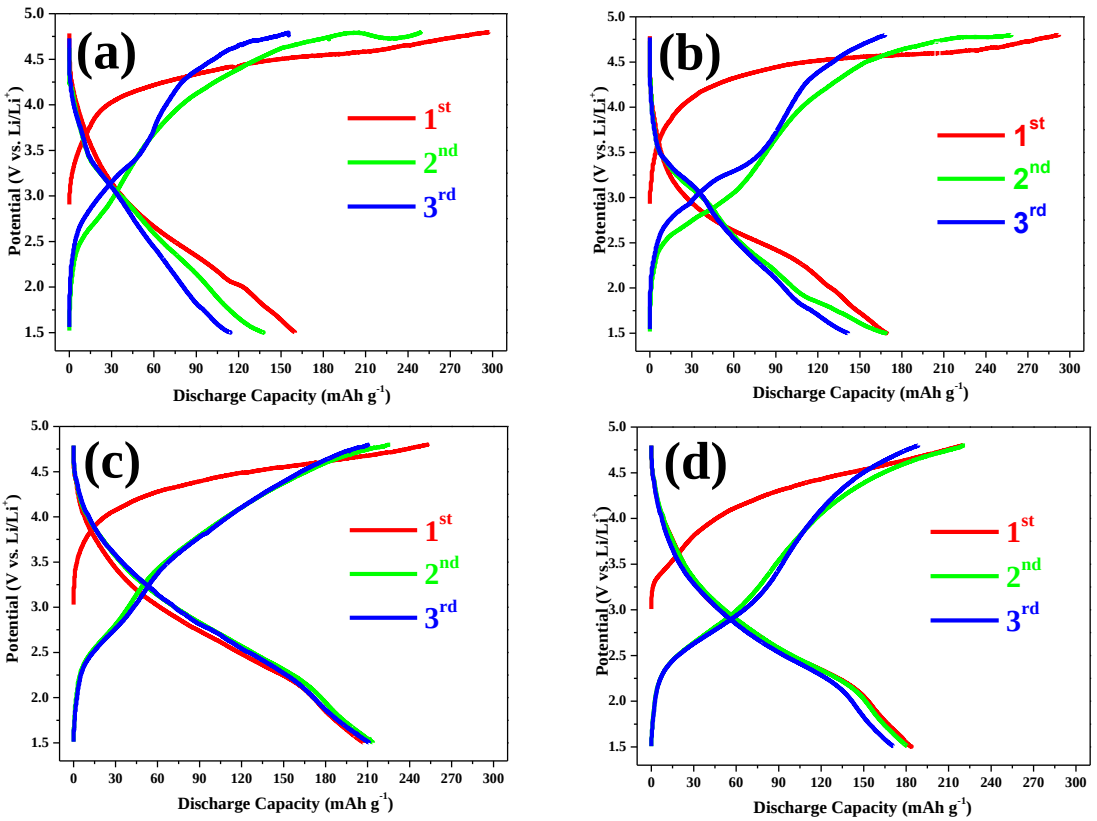

Figure 4. Charge and discharge profiles of (a) $Li_2Mn_{0.5}Fe_{0.5}SiO_4$/C, (b) $Li_2Mn_{0.2}Fe_{0.8}SiO_4$/C, (c) $Li_2Mn_{0.5}Fe_{0.5}SiO_4$/C/pitch, and (d) $Li_2Mn_{0.2}Fe_{0.8}SiO_4$/C/pitch cathode electrodes.

Figure 4 presents the three initial charge and discharge profiles of four cathode electrodes composed of the composite materials. The results revealed that the $Li_2Mn_xFe_{1-x}SiO_4$/C/pitch electrodes exhibited higher discharge capacity and more efficient recycling capacity compared with the untreated electrodes because of their lower D/G ratio, as was determined from Raman measurements. The $Li_2Mn_{0.5}Fe_{0.5}SiO_4$/C/pitch electrode exhibited an initial discharge capacity of 203 mAh g^{-1}, and the $Li_2Mn_{0.2}Fe_{0.8}SiO_4$/C/pitch electrode exhibited an initial discharge capacity of 183 mAh g^{-1}. The different discharge capacities of the two electrodes indicated that a higher concentration of Mn yielded a higher initial capacity in the $Li_2Mn_xFe_{1-x}SiO_4$/C/pitch composite material. Similar results were obtained in the first, second, and third cycles.

Figure 5 illustrates the cycle performance of the four electrodes for 30 cycles. The results revealed that the $Li_2Mn_xFe_{1-x}SiO_4$/C samples without pitch coating delivered a lower discharge capacity compared with the pitch-coated electrodes. The $Li_2Mn_{0.5}Fe_{0.5}SiO_4$/C/pitch electrode delivered a discharge capacity of 203 $mAhg^{-1}$ in the first cycle; however, this had decreased to only 120 mAh g^{-1} in the 30th cycle measurement. Notably, the $Li_2Mn_{0.2}Fe_{0.8}SiO_4$/C/pitch electrode delivered a relatively lower discharge specific capacity of 183 mAh g^{-1} in the first cycle, but this only decreased slightly to 160 mAh g^{-1} in the 30th cycle, which was a cycle retention of approximately 88%. This result indicated that substitution with a higher concentration of Mn in the $Li_2Mn_xFe_{1-x}SiO_4$ compound is detrimental to the cycling stability and that silicate cathode materials with a suitable Mn:Fe

stoichiometry are a potential cathode material for lithium-ion batteries. To elucidate the electrochemical behavior of $Li_2Mn_{0.5}Fe_{0.5}SiO_4$/C/pitch and $Li_2Mn_{0.2}Fe_{0.8}SiO_4$/C/pitch composite materials, CV and EIS analysis were performed.

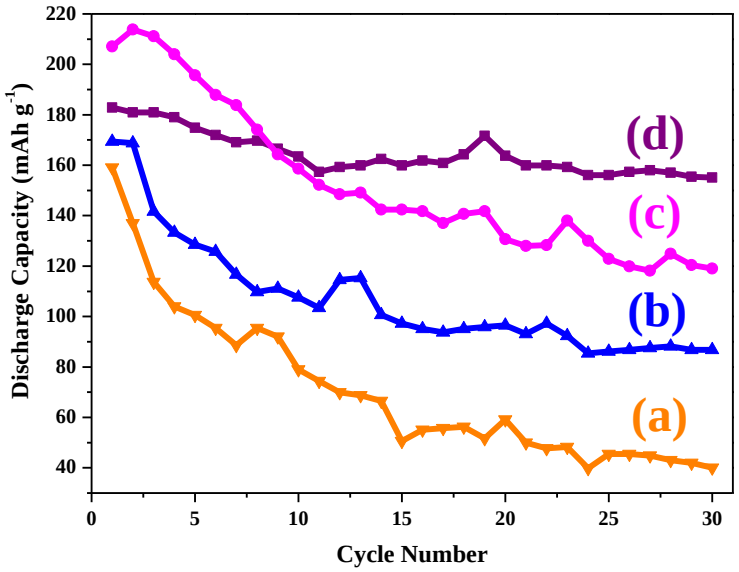

Figure 5. The cycle performance of (a) $Li_2Mn_{0.5}Fe_{0.5}SiO_4$/C, (b) $Li_2Mn_{0.2}Fe_{0.8}SiO_4$/C, (c) $Li_2Mn_{0.5}Fe_{0.5}SiO_4$/C/pitch, and (d) $Li_2Mn_{0.2}Fe_{0.8}SiO_4$/C/pitch cathode electrodes.

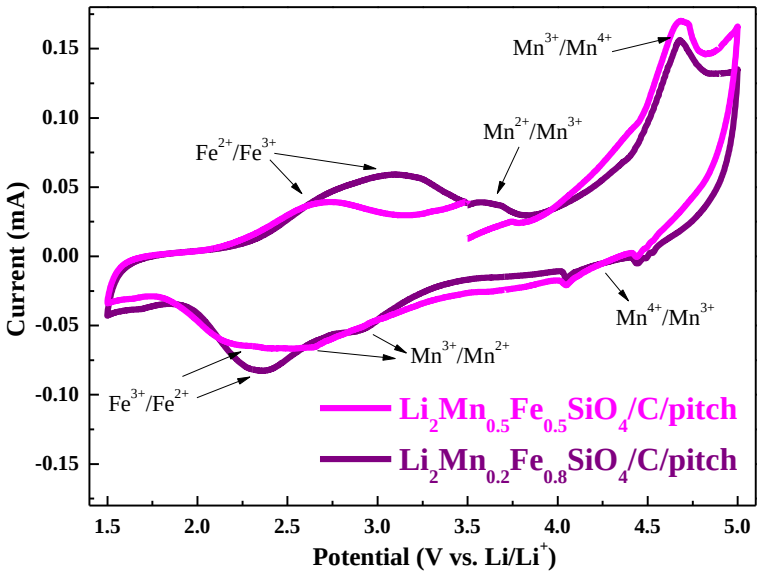

Figure 6. The CV profiles of $Li_2Mn_{0.5}Fe_{0.5}SiO_4$/C/pitch and $Li_2Mn_{0.2}Fe_{0.8}SiO_4$/C/pitch cathode electrodes.

Figure 6 presents the CV profiles of the $Li_2Mn_{0.5}Fe_{0.5}SiO_4$/C/pitch and $Li_2Mn_{0.2}Fe_{0.8}SiO_4$/C/pitch electrodes. The results revealed that these electrodes exhibited a redox pair at a potential of 2.69/2.53 and 3.08/2.33 V, corresponding to Fe^{2+}/Fe^{3+}coupling reaction [31]. The potential differences in these two Fe^{2+}/Fe^{3+} redox couples were calculated as 0.16 and 0.75 V,

respectively, indicating lower polarization of the electrochemical reaction in the $Li_2Mn_{0.5}Fe_{0.5}SiO_4$/C/pitch electrode. However, the sharper redox peaks obtained for the $Li_2Mn_{0.2}Fe_{0.8}SiO_4$/C/pitch electrode indicated more efficient electron transfer than the $Li_2Mn_{0.5}Fe_{0.5}SiO_4$/C/pitch electrode, thus demonstrating a faster kinetic reaction [32]. Furthermore, another two redox couples were discovered. The $Li_2Mn_{0.5}Fe_{0.5}SiO_4$/C/pitch and $Li_2Mn_{0.2}Fe_{0.8}SiO_4$/C/pitch electrodes exhibited almost the same electrochemical behavior in the anodic reaction, corresponding to the Mn^{2+}/Mn^{3+} (3.71 V) and Mn^{3+}/Mn^{4+} (4.69 V) couples. However, the cathodic reaction revealed that Mn substitution triggered different electrochemical behaviors. The Mn^{3+}/Mn^{2+} reaction potential was unclear in the $Li_2Mn_{0.5}Fe_{0.5}SiO_4$/C/pitch electrode and may be 2.66 V, which is lower than the potential (clear, 2.96 V) in the $Li_2Mn_{0.2}Fe_{0.8}SiO_4$/C/pitch electrode. This finding revealed that the $Pmn2_1$ and Pmnb polymorphs of Li_2MnSiO_4 transformed into an amorphous phase during the first Li^+ extraction, and the crystallinity was not recovered after subsequent reduction processes.

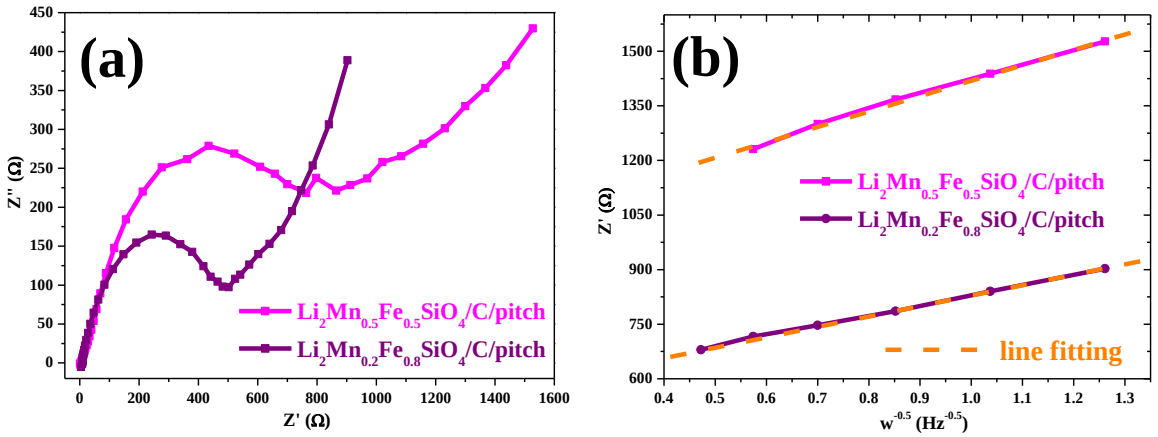

Figure 7. EIS spectra of $Li_2Mn_{0.5}Fe_{0.5}SiO_4$/C/pitch and $Li_2Mn_{0.2}Fe_{0.8}SiO_4$/C/pitch cathode electrodes at 0% SOC. (a) Nyquist plots and (b) The Z' vs. $\omega^{-0.5}$ relationships. The orange dashed line depicted the fitting line of the data on both samples.

Figure 7 presents the EIS spectra of the prepared $Li_2Mn_{0.5}Fe_{0.5}SiO_4$/C/pitch and $Li_2Mn_{0.2}Fe_{0.8}SiO_4$/C/pitch electrodes at 0% SOC after five cycles. All spectra exhibited a semicircle at high frequencies and a straight line at low frequencies. The high-frequency semicircle was related to the resistance of the electrolytic solution (series resistance, R_s) and the current flow caused by the redox reaction at the interface (charge transfer resistance, R_{ct}). The sloping line at the low frequency was associated with lithium diffusion in the solid phase. The $Li_2Mn_{0.2}Fe_{0.8}SiO_4$/C/pitch electrode exhibited an R_{ct} of approximately 571 Ω (Fig. 7a), which was considerably lower than that of the $Li_2Mn_{0.5}Fe_{0.5}SiO_4$/C/pitch electrode (1034 Ω). Furthermore, the lithium-ion diffusion coefficient was calculated from the low-frequency line by using the following equation [33]:

$$D_{Li} = \frac{R^2T^2}{2A^2n^4F^4C^2\sigma^2}, \quad (1)$$

where R is the gas constant (8.314 J mol^{-1} K^{-1}), T is the absolute temperature (298 K at room temperature), A is the surface area of the electrode (1.131 cm^2), n is the number of electrons per molecule during oxidation, F is the Faraday constant (96,485 C mol^{-1}), C is the concentration of lithium ions (mol cm^{-3}), and σ is the Warburg factor (Ω $s^{-0.5}$), which is related to Z_{Re} (Ω) as follows [34]:

$$Z_{Re} = \text{constant} + \sigma\omega^{-0.5}, \quad (2)$$

where ω (Hz) is the angular frequency of the applied sine wave. The relationships between Z_{Re} and the reciprocal square root of angular frequency in the low-frequency region for both samples are displayed in Fig. 7b. The calculation results revealed that the Warburg factors of the $Li_2Mn_{0.5}Fe_{0.5}SiO_4$/C/pitch and $Li_2Mn_{0.2}Fe_{0.8}SiO_4$/C/pitch electrodes after five cycles were 431.4 and 282.8 Ω $s^{-0.5}$, respectively, indicating that the D_{Li} of the $Li_2Mn_{0.2}Fe_{0.8}SiO_4$/C/pitch electrode was almost twice that of the $Li_2Mn_{0.5}Fe_{0.5}SiO_4$/C/pitch cathode. This result indicated that increasing the concentration of Fe substitutions could increase the diffusion coefficient. This is the source of the superiority and higher cycling stability of the $Li_2Mn_{0.2}Fe_{0.8}SiO_4$/C/pitch cathode material relative to the $Li_2Mn_{0.5}Fe_{0.5}SiO_4$/C/pitch cathode material.

DSC measurements were employed to analyze heat flow and thermal reaction with respect to the heating temperature of the prepared $Li_2Mn_{0.5}Fe_{0.5}SiO_4$/C/pitch and $Li_2Mn_{0.2}Fe_{0.8}SiO_4$/C/pitch electrodes. The $Li_2Mn_{0.5}Fe_{0.5}SiO_4$/C/pitch electrode underwent an exothermic reaction at 65.9 °C (Fig. 8). Compared with the $Li_2Mn_{0.2}Fe_{0.8}SiO_4$/C/pitch electrode, the $Li_2Mn_{0.5}Fe_{0.5}SiO_4$/C/pitch electrode exhibited almost no thermal signal response within a similar temperature range. This advantage suggested that the $Li_2Mn_xFe_{1-x}SiO_4$/C composite with higher Fe composition is a more practical choice as the cathode material in lithium-ion batteries to address safety concerns.

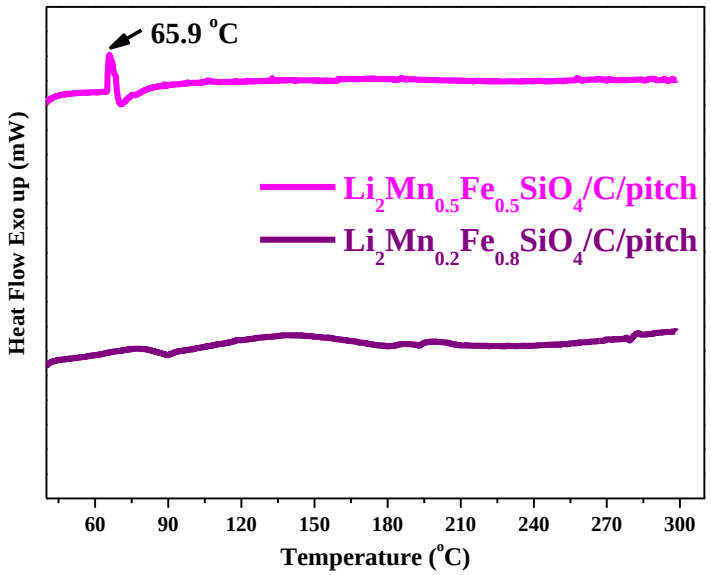

Figure 8. DSC scans of the $Li_2Mn_{0.5}Fe_{0.5}SiO_4$/C/pitch and $Li_2Mn_{0.2}Fe_{0.8}SiO_4$/C/pitch composite materials.

Table 3. The comparisons of literatures and this research.

Materials	Performance	Reference number
Li_2MnSiO_4/C/graphene @0.05C (Solid state method)	220 mAh g^{-1} @ 1st cycle 195 mAh g^{-1} @ 32th cycle	11
Li_2MnSiO_4/PEDOT @0.05C (Supercritical method) @40°C	310 mAh g^{-1} @ 1st cycle 285 mAh g^{-1} @ 2nd cycle	11
Li_2MnSiO_4/C @0.05C (Microwave method) @55°C	250 mAh g^{-1} @ 1st cycle 210 mAh g^{-1} @ 2nd cycle	11
Li_2MnSiO_4 Li_2FeSiO_4	240 mAh g^{-1} 240 mAh g^{-1}	14
Li_2FeSiO_4/CNT@0.05C Li_2MnSiO_4/CNT@0.05C Li_2FeSiO_4/rGO@0.05C Li_2MnSiO_4/rDO@0.05C	105 mAh g^{-1} @ 1st cycle 240 mAh g^{-1} @ 1st cycle 220 mAh g^{-1} @ 1st cycle 230 mAh g^{-1} @ 1st cycle	9
Li_2FeSiO_4 Li_2FeSiO_4/glucose Li_2FeSiO_4/pitch	13 mAh g^{-1} @ 1st cycle 123 mAh g^{-1} @ 1st cycle 132 mAh g^{-1} @ 1st cycle	26
$Li_2Mn_{0.5}Fe_{0.5}SiO_4$/C/pitch @0.0625C	183 mAh g^{-1} @ 1st cycle 160 mAh g^{-1} @ 30th cycle	This research

4. CONCLUSION

This study employed the sol–gel route for synthesizing $Li_2Mn_xFe_{1-x}SiO_4$/C composite materials with efficient electrochemical performance. The synthesized $Li_2Mn_xFe_{1-x}SiO_4$/C composite materials exhibited favorable crystallinity. The carbon content of the pitch-coated $Li_2Mn_xFe_{1-x}SiO_4$/C composite was approximately 40 wt%, and the carbon coating on the surface of the particles provided a high degree of graphitization. SEM revealed that the $Li_2Mn_xFe_{1-x}SiO_4$/C samples were composed of irregularly shaped secondary particles of size ranging from 10 to 60 μm. The discharge capacity of the synthesized pitch-coated $Li_2Mn_{0.2}Fe_{0.8}SiO_4$/C cathode at a rate of 0.1 C was 183 $mAhg^{-1}$ in the first cycle. The capacity retention after the 30th cycle of the $Li_2Mn_{0.2}Fe_{0.8}SiO_4$/C/pitch electrode was 88%. In addition, EIS revealed that a higher Fe concentration in the $Li_2Mn_xFe_{1-x}SiO_4$/C composite material was more effective at reducing the charge transfer resistance of the electrochemical reaction. In conclusion, pitch-coated $Li_2Mn_{0.2}Fe_{0.8}SiO_4$/C ($Li_2Mn_{0.2}Fe_{0.8}SiO_4$/C/pitch) is a potential cathode material for use in lithium-ion batteries and will have practical and commercial applications in the future.

ACKNOWLEDGEMENT
The author is grateful for the financial support from the Ministry of Science and Technology (MOST) of Taiwan, R.O.C, under grant numbers 102-2221-E-011-016-MY3, 104-3113-E-011-002, 104-2745-8-011-001, 105-3113-E-011-002, 105-2628-E-011-005-MY3, 105-2811-E-011-021, 106-3113-E-011-001, 106-2923-E-036-002-MY3.

References

1. M. Arroyo-de Dompablo, M. Armand, J. Tarascon and U. Amador, *Electrochem. Commun.*, 8 (2006) 1292.
2. D. Kempaiah, D. Rangappa and I. Honma, *Chem. Commun.*, 48 (2012) 2698.

3. R. Gummow and Y. He, *J. Power Sources*, 253 (2014) 315.
4. V. Aravindan, K. Karthikeyan, S. Amaresh and Y. Lee, *Electrochem. Solid-State Lett.*, 14 (2011) A33.
5. N. Wagner, A Svensson and F. Vullum-Bruer, *Solid State Ionics*, 276 (2015) 26.
6. S. Aono, T. Tsurudo, K. Urita and I. Moriguchi, *Chem. Commun.*, 49 (2013) 2939.
7. J. Yang, X. Kang, L. Hu, X. Gong, D. He, T. Peng and S. Mu, *J. Alloys Compd.*, 572 (2013) 158.
8. X. Huang, H. Chen, H. Wang, S. Zhou, Y. Chen, B. Liu, J. Yang, G. Zhou, Q. Jiang, M. Qu, Z. Pan and Z. Yu, *Solid State Ionics*, 220 (2012) 18.
9. D. Bhuvaneswari and N. Kalaiselvi, *Dalton Trans.*, 43 (2014) 18097.
10. H. Gong, Y. Zhu, L. Wang, D. Wei, J. Liang and Y. Qian, *J. Power Sources*, 246 (2014) 192.
11. H. Girish and G.Q. Shao, *RSC Adv.*, 5 (2015) 98666.
12. H. Lee, S Park, J. Moon, H. Lee, K. Cho, M. Cho and S. Kim, *Chem. Mater.*, 26 (2014) 3896.
13. S. Zhang, Y. Li, G. Xu, S. Li, Y. Lu, O. Toprakci and X. Zhang, *J. Power Sources*, 213 (2012) 10.
14. H. Sasaki, A. Nemoto, M. Moriya, M. Miyahara, M. Hokazono, S. Katayama, Y. Akimoto, A. Nakajima and S. Hirano, *Ceram. Int.*, 41 (2015) S680.
15. A. Saracibar, Z. Wang, K. J. Carroll, Y. Meng and M. Arroyo-de Dompablo, *J. Mater. Chem. A*, 3 (2015) 6004.
16. R. Dominko, *J. Power Sources*, 184 (2008) 462.
17. G. Mali, M. Rangus, C. Sirisopanaporn and R. Dominko, *Solid State Nucl. Mag. Reson.*, 42 (2012) 33.
18. R. Dominko, I. Arcon, A. Kodre, D. Hanzel and M. Gaberscek, *J. Power Sources*, 189 (2009) 51.
19. Y. Li, W. Sun, J. Liang, H. Sun, I.D. Marco, L. Ni, S. Tang and J. Zhang, *J. Mater. Chem. A*, 4 (2016) 17455.
20. C. Deng, S. Zhang and S. Yang, *J. Alloys Compd.*, 487 (2009) L18.
21. X. Lu, H. Chiu, Z. Arthur, J. Zhou, J. Wang N. Chen, D. Jiang, K. Zaghib and G. Demopoulos, *J. Power Sources*, 329 (2016) 355.
22. H. Kagetama, Y. Hashomoto, Y. Oaki and H. Imai, *CrystEngComm*, 17 (2015) 8486.
23. R. Dominko, D. Conte, D. Hanzel, M. Gaberscek and J. Jamnik, *J. Power Sources*, 178 (2008) 842.
24. Q. Pan, P. Zuo, T. Mu, C. Du, X. Cheng, Y. Ma, Y. Gao and G. Yin, *J. Power Sources*, 347 (2017) 170.
25. Q. Liu, L. Ren, C. Cong, F. Ding, F. Guo, D. Song, J. Guo, X. Shi and L. Zhang, *Electrochem. Acta*, 187 (2016) 264.
26. X. Huang, X. Li, H. Wang, Z. Pan, M. Qu and Z. Yu, *Solid State Ionics*, 181 (2010) 1451.
27. X. Jiang, H. Xu, J. Liu, J. Yang, H. Mao and Y. Qian, *Nano Energy*, 7 (2014) 1.
28. C. Sirisopanaporn, R. Dominko, C. Masquelier, A. Robert Armstrong, G. Maliad and P. Bruce, *J. Mater. Chem.*, 21 (2011) 17823.
29. T. Kaplas and Y. Svirko, *J. Nanophoton.*, 6 (2012) 061703.
30. A. Ferrari, *Solid State Commun.*, 143 (2007) 47.
31. Y. Wang, D. Alsmeyer and R. McCreery, *Chem. Mater.*, 2 (1990) 557.
32. O. Fayemi, A. Adekunle and E. Ebenso, *Sens. Bio-Sens. Res.*, 13 (2017) 17.
33. M. Wang, M. Yang, L. Ma and X. Shen, *RSC Adv.*, 5 (2015) 1612.
34. H. Liu, Q. Cao, L. Fu, C. Li, Y. Wu and H. Wu, *Electrochem. Commun.*, 8 (2006) 1553.